INAF
ISTITUTO NAZIONALE
DI ASTROFISICA
NATIONAL INSTITUTE
FOR ASTROPHYSICS



| | |
|---|---|
| ***Publication Year*** | 2020 |
| ***Acceptance in OA*** | 2025-02-19T12:58:44Z |
| ***Title*** | The first detection of ultra-diffuse galaxies in the Hydra I cluster from the VEGAS survey |
| ***Authors*** | IODICE, ENRICHETTA, CANTIELLO, Michele, Hilker, M., Rejkuba, M., Arnaboldi, M., SPAVONE, MARILENA, GREGGIO, Laura, Forbes, D. A., D'Ago, G., Mieske, S., SPINIELLO, CHIARA, La Marca, A., RAMPAZZO, Roberto, PAOLILLO, Maurizio, Capaccioli, M., SCHIPANI, Pietro |
| ***Publisher's version (DOI)*** | 10.1051/0004-6361/202038523 |
| ***Handle*** | http://hdl.handle.net/20.500.12386/36054 |
| ***Journal*** | ASTRONOMY & ASTROPHYSICS |
| ***Volume*** | 642 |

A&A 642, A48 (2020)
https://doi.org/10.1051/0004-6361/202038523
© ESO 2020

Astronomy & Astrophysics

# The first detection of ultra-diffuse galaxies in the Hydra I cluster from the VEGAS survey

E. Iodice[1,2], M. Cantiello[3], M. Hilker[2], M. Rejkuba[2], M. Arnaboldi[2], M. Spavone[1], L. Greggio[4], D. A. Forbes[5], G. D'Ago[6], S. Mieske[7], C. Spiniello[1,8], A. La Marca[9], R. Rampazzo[10], M. Paolillo[1,9,11], M. Capaccioli[1,9], and P. Schipani[1]

[1] INAF – Astronomical Observatory of Capodimonte, Salita Moiariello 16, 80131 Naples, Italy
e-mail: enrichetta.iodice@inaf.it
[2] European Southern Observatory, Karl-Schwarzschild-Strasse 2, 85748 Garching bei Muenchen, Germany
[3] INAF-Astronomical Abruzzo Observatory, Via Maggini, 64100 Teramo, Italy
[4] INAF – Osservatorio Astronomico di Padova, Vicolo dell'Osservatorio 5, 35122 Padova, Italy
[5] Centre for Astrophysics and Supercomputing, Swinburne University of Technology, Hawthorn, Victoria 3122, Australia
[6] Instituto de Astrofísica, Facultad de Física, Pontificia Universidad Católica de Chile, Av. Vicuña Mackenna 4860, 7820436 Macul, Santiago, Chile
[7] European Southern Observatory, Alonso de Cordova 3107, Vitacura, Santiago, Chile
[8] Department of Physics, University of Oxford, Denys Wilkinson Building, Keble Road, Oxford OX1 3RH, UK
[9] University of Naples "Federico II", C.U. Monte Sant'Angelo, Via Cinthia, 80126 Naples, Italy
[10] INAF – Astronomical Observatory of Padova, Via dell'Osservatorio 8, 36012 Asiago, VI, Italy
[11] INFN, Sezione di Napoli, Napoli 80126, Italy

Received 28 May 2020 / Accepted 21 July 2020

**ABSTRACT**

In this paper, we report the discovery of 27 low-surface brightness galaxies, of which 12 are candidates for ultra-diffuse galaxies (UDG) in the Hydra I cluster, based on deep observations taken as part of the VST Early-type Galaxy Survey (VEGAS). This first sample of UDG candidates in the Hydra I cluster represents an important step in our project that aims to enlarge the number of confirmed UDGs and, through study of statistically relevant samples, constrain the nature and formation of UDGs. This study presents the main properties of this class of galaxies in the Hydra I cluster. For all UDGs, we analysed the light and colour distribution, and we provide a census of the globular cluster (GC) systems around them. Given the limitations of a reliable GC selection based on two relatively close optical bands only, we find that half of the UDG candidates have a total GC population consistent with zero. Of the other half, two galaxies have a total population larger than zero at $2\sigma$ level. We estimate the stellar mass, the total number of GCs, and the GC specific frequency ($S_N$). Most of the candidates span a range of stellar masses of $10^7-10^8\,M_\odot$. Based on the GC population of these newly discovered UDGs, we conclude that most of these galaxies have a standard or low dark matter content, with a halo mass of $\leq 10^{10}\,M_\odot$.

**Key words.** galaxies: clusters: individual: Hydra I – galaxies: photometry – galaxies: dwarf – galaxies: formation

## 1. Introduction

Ultra-diffuse galaxies (UDGs) are extreme low surface brightness (LSB) objects ($\mu_g \geq 24$ mag arcsec$^{-2}$) with effective radii comparable to that of large spirals, but stellar masses similar to dwarf galaxies ($\sim 10^7-10^8\,M_\odot$). Renewed interest in the LSB objects and the definition of a new class of galaxies as UDGs comes from the discovery of a significant population of these rather extreme objets in the Coma cluster (van Dokkum et al. 2015; Koda et al. 2015). Recent works report the discovery of UDGs also in less dense environments as groups of galaxies and in the field (Román & Trujillo 2017; van der Burg et al. 2017; Shi et al. 2017; Müller et al. 2018; Prole et al. 2019b; Forbes et al. 2019, 2020b).

The nature and origin of the UDGs are still debated. Ultra-diffuse galaxies could be 'failed' galaxies, which lost their gas supply at early epochs. If so, the UDG should posses a massive dark matter (DM) halo to survive in dense environments like galaxy clusters (van Dokkum et al. 2015). Some theoretical models explain UDGs as extreme dwarf galaxies, whose large size could be due to high spins in DM halos (Amorisco & Loeb 2016; Rong et al. 2017; Tremmel et al. 2019) or to tidal interactions (e.g. Yozin & Bekki 2015). Di Cintio et al. (2017) proposed that very extended UDG-like systems could have been formed by the kinematical heating of their stars as consequence of internal processes (i.e. gas outflows associated with feedback).

Populations of UDGs have been reproduced in cosmological galaxy simulations both in galaxy clusters (e.g. Sales et al. 2020) and in low-density environments (e.g. Wright et al. 2020). They suggested that two classes of UDGs might exist: one, found in the field, defined as normal LSB galaxies, and a second class of UDGs, near cluster centres, which shaped their large size and low surface brightness by the cluster tidal forces.

From the observational side, given the very low surface brightness, the detection and analysis of UDGs is challenging. Some UDGs in Coma and Virgo clusters appear to host a large number of globular clusters (GCs) for their luminosity, indicating that they may be DM-dominated. This might support

the failed galaxies hypothesis (Beasley et al. 2016; Peng & Lim 2016; van Dokkum et al. 2016, 2019b; Forbes et al. 2020a). On the other hand, other works showed that UDGs can have stellar masses and DM content consistent with dwarf galaxies, suggesting that they could be extremely extended dwarfs (Beasley & Trujillo 2016; Amorisco 2018; Alabi et al. 2018; Ferré-Mateu et al. 2018). Furthermore, some UDGs are found with very low DM content (van Dokkum et al. 2016, 2019a; Danieli et al. 2019; Prole et al. 2019a).

From the analysis of the average colours, two populations of UDGs were identified: red and quenched UDGs, which occupy the red sequence (van Dokkum et al. 2015; van der Burg et al. 2017), and a blue population of UDGs, which are mostly found in the field (e.g. Leisman et al. 2017; Román & Trujillo 2017; Prole et al. 2019b). The spatial distribution of UDGs inside their host environment seems to be asymmetric, meaning overdensities of UDGs are found close to sub-structures, as subgroups of galaxies, which are falling into the cluster (van der Burg et al. 2017; Janssens et al. 2019).

The few spectroscopic data acquired for UDGs find both metal poor ($-0.5 \leq [M/H] \leq -1.5$) and old systems ($t \sim 9$ Gyr, e.g. Fensch et al. 2019; Ferré-Mateu et al. 2018; Gu et al. 2018; Ruiz-Lara et al. 2018), as well as younger UDGs with an extended star formation history and massive DM halo (Martín-Navarro et al. 2019).

The available data show that UDGs span a wide range of properties, which do not fit in a unique formation scenario, and clearly indicate that, to date, our knowledge of UDGs is still poorly constrained. The main issues that need to be tackled are: (i) whether or not two classes of UDGs exist, one being extreme cases of dwarf galaxies and the other as pure UDGs, with distinct formation scenarios, structural parameters and photometric properties; and (ii) what is the fraction of baryonic versus DM content in UDGs, and does this fraction differ for the two putative classes? If the majority of UDGS proves to be without DM, then the current paradigm of galaxy formation should be revised and better understood in the specific parameter space occupied these galaxy systems.

In this paper, we report the discovery of 12 UDG candidates in the Hydra I cluster. This is a rich environment of galaxies located at ~51 Mpc (Christlein & Zabludoff 2003), with a virial mass of $\sim 2 \times 10^{14}\, M_{\odot}$ (Girardi et al. 1998), from which we derived a virial radius $R_{\rm vir} \sim 1.6$ Mpc. The cluster core is dominated by the two brightest early-type galaxies, NGC 3309 and NGC 3311, embedded in an extended diffuse stellar halo (Arnaboldi et al. 2012). Most of the recent studies of Hydra I focused on the light distribution and kinematics in the cluster core, which showed the presence of ongoing interactions and traced the extended mass assembly around NGC 3311 (Ventimiglia et al. 2011; Richtler et al. 2011; Coccato et al. 2011; Misgeld et al. 2008, 2011; Arnaboldi et al. 2012; Koch et al. 2012; Barbosa et al. 2018; Hilker et al. 2018). We carried out the first search for UDGs enabled by a new wide area and deep-imaging dataset.

## 2. Observations and data analysis

The Hydra I cluster is a target of the VST Early-type Galaxy Survey (VEGAS[1]), a multi-band ($u, g, r, i$), deep imaging survey carried out with the European Southern Observatory (ESO) VLT Survey Telescope (VST). The VST is a 2.6 m wide field optical telescope (Schipani et al. 2012), equipped with OmegaCAM, a $1^{\circ} \times 1^{\circ}$ camera with a resolution of 0.21 arcsec pixel$^{-1}$. The imaging data for the Hydra I cluster, presented in this work, were collected in the $g$ and $r$ bands, in dark time, with total integration times of 2.8 and 3.22 hours, respectively. The measured image quality had an average $FWHM \sim 0.8$ arcsec. Data were acquired with the step dither observing strategy, consisting of a cycle of short exposures (~150 s) on the science target and on an adjacent field (close in space and time) to the science frame. This strategy was also adopted for other VEGAS targets (Spavone et al. 2018; Iodice et al. 2020) and for the Fornax Deep Survey (FDS, Iodice et al. 2016, 2019; Venhola et al. 2018). It certifies a very accurate estimate of the sky background. For the Hydra I dataset, a 7-magnitude bright star falls on the NE side of the cluster core, and was always put in one of the two wide OmegaCAM gaps during observations, to reduce the scattered light.

The data reduction was performed using *VST-Tube*, which is one of the dedicated pipelines to process OmegaCAM observations (Grado et al. 2012; Capaccioli et al. 2015). For the final stacked images we estimated surface brightness depths[2] of $\mu_g = 28.6 \pm 0.2$ mag and $\mu_r = 28.1 \pm 0.2$ mag in the $g$ and $r$ bands, respectively. The light of the two bright stars close to the cluster core was modelled and subtracted from the reduced images.

The final VST mosaic extends over $1^{\circ} \times 2^{\circ}$ ($0.9 \times 1.8$ Mpc), which covers the cluster out to the virial radius (~1.6 Mpc). A portion of the mosaic centred on the cluster core is shown in Fig. 1. By visual inspection of this area, looking for faint, diffuse, and extended objects, we identified 27 LSB galaxies that are not included in previous catalogues (Christlein & Zabludoff 2003; Misgeld et al. 2008), since they are below the detection limits of such studies (see Sect. 3). All 27 identified LSB candidates are marked with black circles in Fig. 1.

For each LSB candidate, we (i) extracted a thumbnail from the mosaic (three times more extended than the target) where all bright stars are modelled and subtracted, while the remaining fainter sources are masked, and a residual local background is subtracted; (ii) performed the isophote fitting using the IRAF task ELLIPSE, to obtain the azimuthally averaged $g$ and $r$-band surface brightness profiles, the total magnitudes, and the average colours; ( iii) derived the 2D fit of the galaxy light, in the $g$ band using GALFIT (Peng et al. 2010) and adopting a single Sersic function, with all structural parameters left free. All LSB galaxies are on average 10–100 times more extended than the FWHM of the point-spread function, therefore we discarded the convolution step in the modelling and simply excluded the central regions affected by the seeing disc (≤1 arcsec).

### 2.1. Identification of UDGs

Assuming a distance of 51 ± 6 Mpc (Christlein & Zabludoff 2003), we adopted the van Dokkum et al. (2015) selection criteria (i.e. $R_{\rm e} \geq 1.5$ kpc and $\mu_0 \geq 24$ mag/arcsec$^2$ in $g$ band) to identify UDG candidates from the list of 27 LSB galaxies. Taking into account the error estimates for $\mu_0$ and $R_{\rm e}$[3], we found nine objects falling in the $\mu_0 - R_{\rm e}$ region consistent with UDGs, and an additional three galaxies that cross the lower limit for the $R_{\rm e}$ value, considering the uncertainty on the distance ($\Delta R_{\rm e} \simeq 0.12$ kpc). To be as comprehensive as possible, we also included these objects since they are consistent with the selection criteria within the uncertainties. Therefore, the final list is made

[1] see http://www.na.astro.it/vegas/VEGAS/Welcome.html

[2] Derived as the flux corresponding to $5\sigma$, with $\sigma$ estimated over an empty area of 1 arcsec.

[3] The error estimates on $\mu_0$ and $R_{\rm e}$ take into account the uncertainties on the fitting, which are about 0.2% and 6%, respectively, and on the sky removal for $\mu_0$ (~1%) and on the distance (~12%) for $R_{\rm e}$.

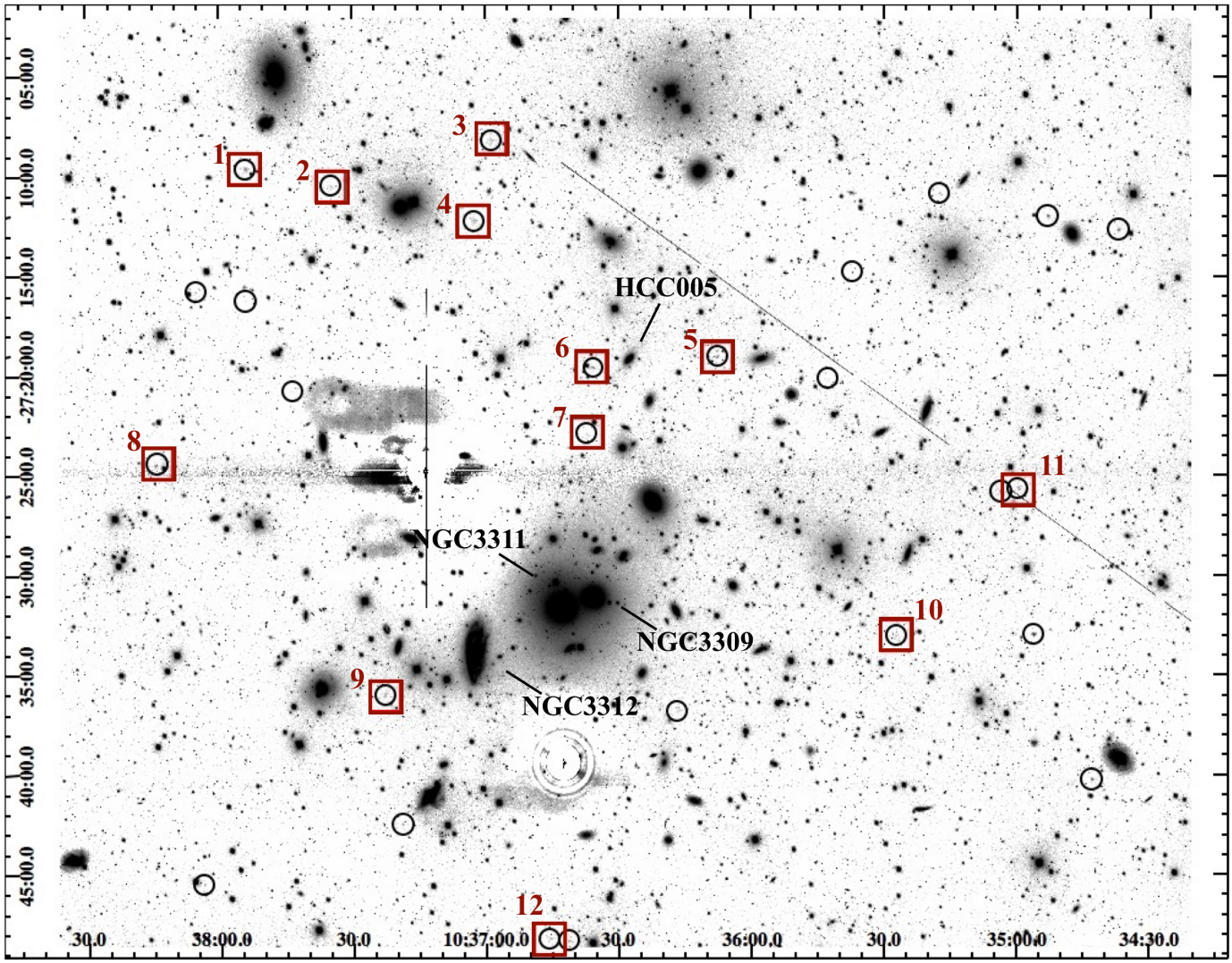


**Fig. 1.** VST mosaic ($56.7 \times 46.55' \sim 0.8 \times 0.7$ Mpc) of the Hydra I cluster in the $g$ band, which correspond to $\sim 0.5 R_{\rm vir}$. NGC 3311 and NGC 3309 are the two brightest cluster galaxies located close to the image centre, embedded in the extended diffuse light envelope. The 27 LSB galaxies detected in this work are marked as black circles. Red squares show the UDGs. North is up and east is on the left.

**Table 1.** Parameters of the UDG candidates in the Hydra I cluster.

| Object | RA J2000 | Dec J2000 | $M_r$ [mag] | $g-r$ [mag] | $M/L$ | $M_*$ [$10^8\,M_\odot$] | $\mu_0$ [mag arcsec$^{-2}$] | $R_{\rm e}$ [kpc] | $n$ | $q$ |
|---|---|---|---|---|---|---|---|---|---|---|
| Hydra I-UDG 1 | 10:37:54.12 | −27:09:37.50 | $-15.48 \pm 0.07$ | $0.40 \pm 0.09$ | 0.90 | 1.12 | $24.20 \pm 0.10$ | $1.75 \pm 0.12$ | $0.621 \pm 0.005$ | $0.766 \pm 0.003$ |
| Hydra I-UDG 2 | 10:37:34.89 | −27:10:29.94 | $-14.27 \pm 0.05$ | $0.53 \pm 0.2$ | 1.35 | 0.55 | $24.97 \pm 0.08$ | $1.55 \pm 0.12$ | $0.72 \pm 0.01$ | $0.877 \pm 0.007$ |
| Hydra I-UDG 3 | 10:36:58.63 | −27:08:10.21 | $-14.7 \pm 0.2$ | $0.75 \pm 0.3$ | 2.71 | 1.65 | $25.2 \pm 0.2$ | $1.88 \pm 0.12$ | $0.572 \pm 0.013$ | $0.79 \pm 0.01$ |
| Hydra I-UDG 4 | 10:37:02.64 | −27:12:15.01 | $-16.03 \pm 0.04$ | $0.95 \pm 0.10$ | 5.11 | 10.6 | $24.86 \pm 0.05$ | $2.64 \pm 0.12$ | $0.597 \pm 0.006$ | $0.748 \pm 0.003$ |
| Hydra I-UDG 5 | 10:36:07.68 | −27:19:03.26 | $-14.66 \pm 0.09$ | $0.65 \pm 0.14$ | 1.98 | 1.16 | $23.7 \pm 0.3$ | $1.42 \pm 0.12$ | $0.89 \pm 0.01$ | $0.582 \pm 0.004$ |
| Hydra I-UDG 6 | 10:36:35.80 | −27:19:36.12 | $-14.38 \pm 0.08$ | $0.32 \pm 0.2$ | 0.70 | 0.32 | $24.08 \pm 0.13$ | $1.37 \pm 0.12$ | $0.706 \pm 0.006$ | $0.629 \pm 0.002$ |
| Hydra I-UDG 7 | 10:36:37.16 | −27:22:54.93 | $-13.72 \pm 0.13$ | $0.6 \pm 0.3$ | 1.98 | 0.49 | $24.37 \pm 0.4$ | $1.66 \pm 0.12$ | $1.32 \pm 0.03$ | $0.73 \pm 0.01$ |
| Hydra I-UDG 8 | 10:38:14.59 | −27:24:27.07 | $-14.87 \pm 0.07$ | $0.34 \pm 0.13$ | 0.74 | 0.53 | $23.22 \pm 0.6$ | $1.40 \pm 0.12$ | $0.98 \pm 0.02$ | $0.578 \pm 0.005$ |
| Hydra I-UDG 9 | 10:37:22.85 | −27:36:02.80 | $-15.16 \pm 0.12$ | $0.6 \pm 0.2$ | 1.92 | 1.78 | $24.2 \pm 0.2$ | $3.46 \pm 0.12$ | $1.38 \pm 0.01$ | $0.54 \pm 0.01$ |
| Hydra I-UDG 10 | 10:35:27.32 | −27:33:03.86 | $-13.89 \pm 0.08$ | $0.4 \pm 0.2$ | 0.90 | 0.26 | $24.33 \pm 0.3$ | $2.29 \pm 0.10$ | $1.53 \pm 0.02$ | $0.90 \pm 0.01$ |
| Hydra I-UDG 11 | 10:35:04.16 | −27:26:17.26 | $-14.75 \pm 0.07$ | $0.43 \pm 0.11$ | 0.99 | 0.63 | $24.36 \pm 0.13$ | $1.66 \pm 0.12$ | $0.80 \pm 0.01$ | $0.92 \pm 0.01$ |
| Hydra I-UDG 12 | 10:34:59.55 | −27:25:37.95 | $-14.3 \pm 0.2$ | $0.8 \pm 0.4$ | 2.8 | 1.19 | $25.1 \pm 0.2$ | $1.64 \pm 0.12$ | $0.67 \pm 0.02$ | $0.72 \pm 0.01$ |

**Notes.** Column 1 reports the name of the UDG candidate. In Cols. 2 and 3 we list the coordinates of the UDGs. In Cols. 4 and 5 are reported the total $r$-band magnitude and the average $g-r$ colour. Columns 6 and 7 give the stellar mass-to-light ratio and stellar mass, respectively, derived in the $r$ band. Columns 8–11 list the structural parameters derived from the 2D fit in the $g$ band: the central surface brightness, the effective radius in kpc, the $n$ exponent of the Sérsic law and the axial ratio, respectively. Magnitudes and colours are corrected for Galactic extinction using values from Schlegel et al. (1998).

**Table 2.** LSB candidates in the Hydra I cluster.

| Object | RA J2000 | Dec J2000 | $M_r$ [mag] | $g-r$ [mag] | $\mu_0$ [mag arcsec$^{-2}$] | $R_e$ [kpc] | $n$ | $q$ |
|---|---|---|---|---|---|---|---|---|
| Hydra I-LSB 1 | 10:35:17.540 | −27:10:51.96 | −13.31 ± 0.14 | 1.1 ± 0.4 | 24.2 ± 0.3 | 0.86 ± 0.12 | 1.05 ± 0.02 | 0.713 ± 0.009 |
| Hydra I-LSB 2 | 10:34:53.099 | −27:12:00.06 | −15.12 ± 0.04 | 0.69 ± 0.09 | 23.57 ± 0.13 | 1.08 ± 0.12 | 0.69 ± 0.004 | 0.903 ± 0.003 |
| Hydra I-LSB 3 | 10:34:37.181 | −27:12:41.14 | −14.55 ± 0.09 | 0.34 ± 0.15 | 23.73 ± 0.14 | 0.997 ± 0.12 | 0.660 ± 0.004 | 0.979 ± 0.003 |
| Hydra I-LSB 4 | 10:35:37.232 | −27:14:50.14 | −14.25 ± 0.05 | 0.58 ± 0.12 | 23.5 ± 0.2 | 0.62 ± 0.12 | 0.580 ± 0.005 | 0.925 ± 0.003 |
| Hydra I-LSB 5 | 10:37:54.147 | −27:16:15.31 | −13.64 ± 0.11 | 0.4 ± 0.2 | 25.65 ± 0.14 | 1.29 ± 0.12 | 0.58 ± 0.02 | 0.858 ± 0.013 |
| Hydra I-LSB 6 | 10:38:05.430 | −27:15:46.89 | −14.08 ± 0.06 | 0.60 ± 0.11 | 24.0 ± 0.2 | 1.02 ± 0.12 | 0.882 ± 0.012 | 0.763 ± 0.006 |
| Hydra I-LSB 7 | 10:37:43.555 | −27:20:44.73 | −13.19 ± 0.05 | 0.55 ± 0.11 | 25.00 ± 0.15 | 1.21 ± 0.12 | 0.63 ± 0.02 | 0.55 ± 0.01 |
| Hydra I-LSB 8 | 10:35:42.806 | −27:20:09.61 | −12.35 ± 0.13 | 0.4 ± 0.2 | 25.60 ± 0.13 | 0.92 ± 0.13 | 0.78 ± 0.03 | 0.94 ± 0.02 |
| Hydra I-LSB 9 | 10:36:16.856 | −27:36:50.83 | −13.01 ± 0.09 | 0.7 ± 0.2 | 25.12 ± 0.12 | 1.00 ± 0.12 | 0.73 ± 0.02 | 0.63 ± 0.01 |
| Hydra I-LSB 10 | 10:35:03.551 | −27:25:50.07 | −14.46 ± 0.10 | 0.9 ± 0.3 | 23.6 ± 0.2 | 0.98 ± 0.12 | 0.609 ± 0.006 | 0.675 ± 0.003 |
| Hydra I-LSB 11 | 10:34:56.212 | −27:32:57.79 | −15.32 ± 0.07 | 0.29 ± 0.09 | 22.86 ± 0.15 | 1.14 ± 0.12 | 0.765 ± 0.003 | 0.834 ± 0.001 |
| Hydra I-LSB 12 | 10:38:03.959 | −27:45:28.18 | −14.40 ± 0.05 | 0.9 ± 0.2 | 24.3 ± 0.2 | 1.28 ± 0.12 | 0.627 ± 0.011 | 0.484 ± 0.004 |
| Hydra I-LSB 13 | 10:37:19.034 | −27:42:29.29 | −13.95 ± 0.07 | 0.62 ± 0.14 | 24.53 ± 0.14 | 1.08 ± 0.12 | 0.56 ± 0.01 | 0.653 ± 0.006 |
| Hydra I-LSB 14 | 10:36:41.231 | −27:48:20.04 | −13.85 ± 0.08 | 1.0 ± 0.4 | 24.0 ± 0.3 | 1.03 ± 0.12 | 0.81 ± 0.01 | 0.546 ± 0.005 |
| Hydra I-LSB 15 | 10:34:42.961 | −27:40:14.42 | −14.96 ± 0.10 | 0.6 ± 0.2 | 23.1 ± 0.2 | 0.89 ± 0.12 | 0.795 ± 0.004 | 0.920 ± 0.003 |

**Notes.** Column 1 reports the name of the LSB candidate, and in Cols. 2 and 3 we list the coordinates. In Cols. 4 and 5, the total $r$-band magnitude and the average $g-r$ colour are reported. Columns 6 and 9 list the structural parameters derived from the 2D fit in the $g$ band: the central surface brightness, the effective radius in kpc, the $n$ exponent of the Sersic law, and the axial ratio, respectively. Magnitudes and colours are corrected for Galactic extinction using values from Schlegel et al. (1998).

of 12 UDG candidates and is given in Table 1. All remaining LSB galaxies are listed in Table 2. In both tables we include the total luminosity, colours, and structural parameters. The location of the selected UDGs inside the cluster is displayed in Fig. 1 with red boxes, and the cutout of each UDG is shown in Figs. 2 and 3. The azimuthally averaged surface brightness profiles for the UDG candidates and the relative best fits are shown in Fig. 4.

### 2.2. Detection of the globular clusters in UDGs

To identify GCs around the UDGs, we applied the same strategy already used in other works based on VST data, where a combination of the detected sources' magnitude, colours, and shape parameters is adopted to identify GC candidates (Cantiello et al. 2015, 2018a, 2020). Briefly, we proceeded as follows. We first ran SExtractor (Bertin & Arnouts 1996) on image cutouts centred on UDG, with size $\sim 10 \times R_e$ on each side. To improve source detection and deblending down to the faintest magnitude level, the galaxy model derived from GALFIT was subtracted from both the $g$ and $r$ frames. For each source we derived the automated aperture magnitude based on Kron (1980) first moment algorithms (SExtractor MAG_AUTO$_X$, where $X$ refers to the $g$- or the $r$-band), and the aperture magnitude within 4 and 6 pixels diameters (MAG_APER$_X$). We used MAG_AUTO$_X$ to estimate the total magnitude of the source, while the aperture magnitudes is adopted for the $g-r$ colour MAG_APER$_g$(6pixel)−MAG_APER$_r$(6pixel) of the source, and the concentration index (CI$_X$ = MAG_APER$_X$(4pixel)−MAG_APER$_X$(6pixel)), which is an indicator of source compactness (Peng et al. 2011).

At the adopted distance of Hydra I, the turnover magnitude (TOM) of the GC luminosity function (GCLF) is $\mu_{g,\mathrm{TOM}} \sim 26.0$ mag (e.g. Villegas et al. 2010) and $\mu_{r,\mathrm{TOM}} \sim 25.4$ mag, based on a median $\langle g-r \rangle \sim 0.6$ (mag) for the GC population (Cantiello et al. 2018b). The TOM in both bands roughly matches with the image limiting magnitude, defined as the $5\sigma$ AB magnitude, which is determined from the median S/N estimated as $\Delta\mathrm{MAG\_AUTO}_X^{-1}$.

To identify GC candidates, we selected sources with the following characteristics: (i) $g$ band magnitude between 23.5 and 26 mag, meaning the expected range between the TOM and $3\sigma_{\mathrm{GCLF}}$ mag brighter (Villegas et al. 2010); (ii) colour within the interval $0.25 \leq g-r \leq 1.25$ mag; (iii) SExtractor CLASS_STAR $\geq 0.4$; (iv) elongation, i.e. major-to-minor axis ratio ≤2 in both bands; (v) concentration index within ∼0.1 mag of the sequence of local point sources (see Cantiello et al. 2020, for more details).

In order to select the GC members of each UDG, we need to correct for the contamination of the sample due to foreground stars, background compact galaxies, and possible intra-cluster GCs. This is most effectively achieved by estimating the local contamination in the spatial regions between $5 \leq R_e \leq 10$ around each UDG candidate. The number of contaminants subtracted from the sample of GCs selected in each galaxy is on average $3.3 \pm 0.8$ arcmin$^{-2}$.

We obtained two different estimates of the total number of GCs ($N_{\mathrm{GC}}$). Adopting the approach suggested by van Dokkum et al. (2016), we estimated the total population within $1.5R_e$. In addition, the total number of GCs within $5\,R_e$, which is the upper limit for bound systems (Kartha et al. 2014; Forbes 2017; Caso et al. 2019), is also derived. Since the photometry reaches roughly the TOM peak, and assuming that the GCLF is also a Gaussian for the UDGs (e.g. Hanes 1977; Rejkuba 2012; van Dokkum et al. 2016), we derived $N_{\mathrm{GC}}$ as twice the background corrected GC density over the $5\,R_e$ area of the UDG, times the area. The only difference with the $N_{\mathrm{GC}}$ within $1.5\,R_e$ is that it is assumed that only half of the GC population is within $1.5\,R_e$, hence the total population is estimated as four times the background corrected GC density over $1.5\,R_e$ area, times the area.

We also estimated the GC background level in three independent fields located outside the virial radius of the cluster, ∼17.5′ wide on each side, by running the same detection and selection procedures outlined above. The estimated GC background density obtained is $\rho_{\mathrm{GC\ background}} = 1.27 \pm 0.10$ arcmin$^{-2}$, a value either consistent with the background around the UDGs, or lower than that, indicating the presence of GCs contaminants from close GC systems of major galaxies or due to intra-cluster GCs. We verified that the level of foreground contamination by Milky Way stars in the direction of Hydra I is ∼50% of the

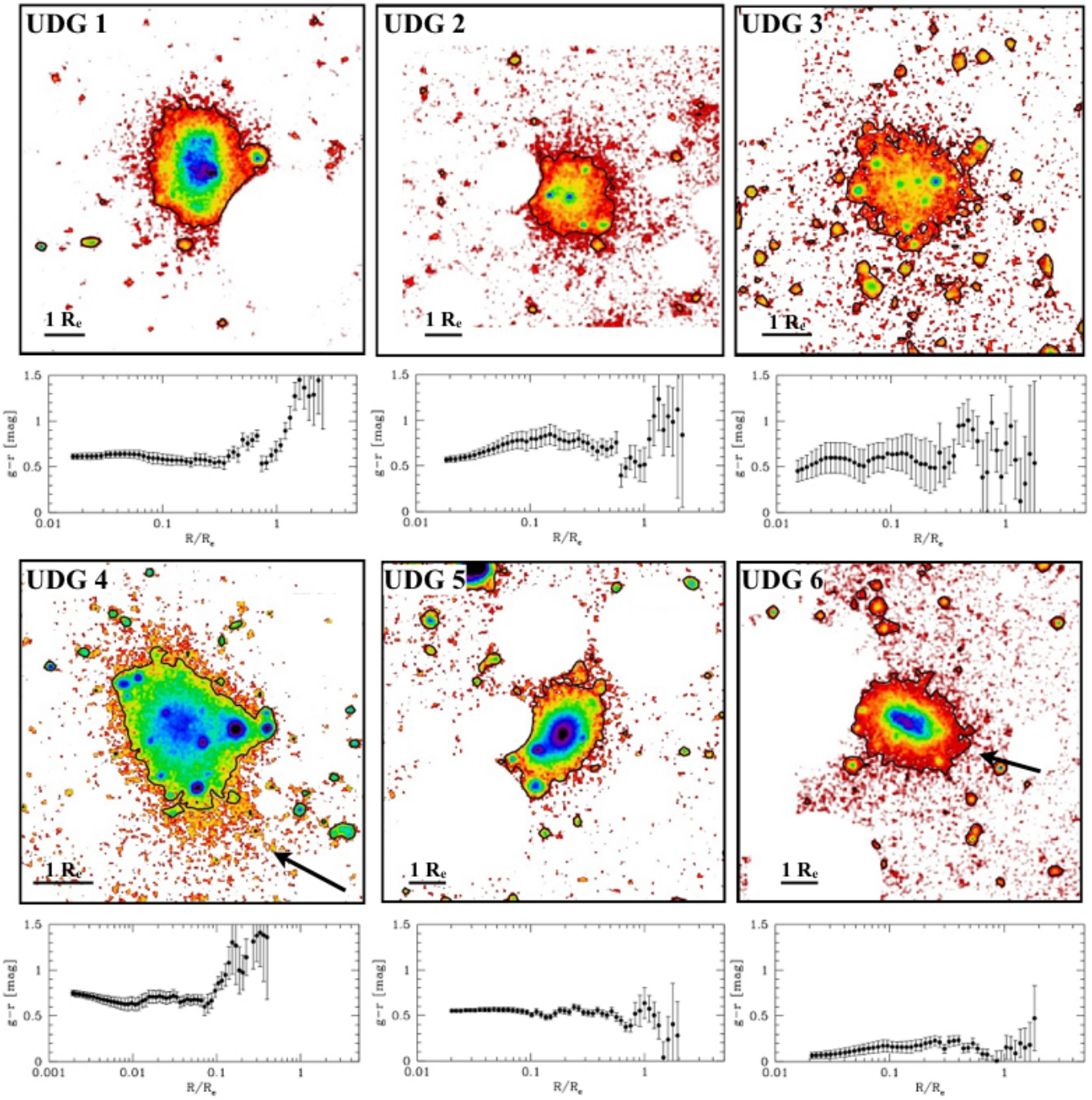


**Fig. 2.** Images of the UDG candidates in the $g$ band in flux levels. The black contour indicates the surface brightness level of $\mu_g = 27$ mag arcsec$^{-2}$. In the lower left corner we show the $R_e$ length. The field of view of all boxes is 1 × 1 arcmin (~14.9 kpc). The black arrow in the image of UDG 4 and UDG 6 indicates the tidal features described in the text. The area that was masked due to contaminating stars is shown as white (circular) background. Below each image we plot the $g-r$ colour profile of the relative UDG.

number we estimated from real data, by using both the TRILEGAL and Besancon models (Girardi et al. 2005; Robin et al. 2003).

The uncertainty on $N_{GC}$ is derived by propagating a 20% error on the adopted scaling factors (i.e. two for $N_{GC}$ at $5\,R_e$, and four at $1.5\,R_e$, respectively), 10% for the error on the density of background sources (slightly larger than the rms from the three background fields outside the cluster core), and 20% contamination on the density of GC candidates over the UDG area. The two $N_{GC}$ estimates agree within the adopted uncertainties and they are listed in Table 3. We found that six UDGs have $N_{GC}$ consistent with zero, independently from the approach adopted to estimate it. Two out of the 12 galaxies (UDG 3 and UDG 11) have $N_{GC}$ different from zero at $>2\sigma$ level. One object (UDG 4) has $N_{GC}$ different from zero at only $1\sigma$ for both estimates. All other UDGs in the sample have $N_{GC}$ between 1 and 2 $\sigma$ different than zero, depending on the approach used (UDG 2, UDG 7, UDG 9).

The total number of GCs is used to estimate (i) the total halo mass $M_h$ for those UDGs with a significant number of

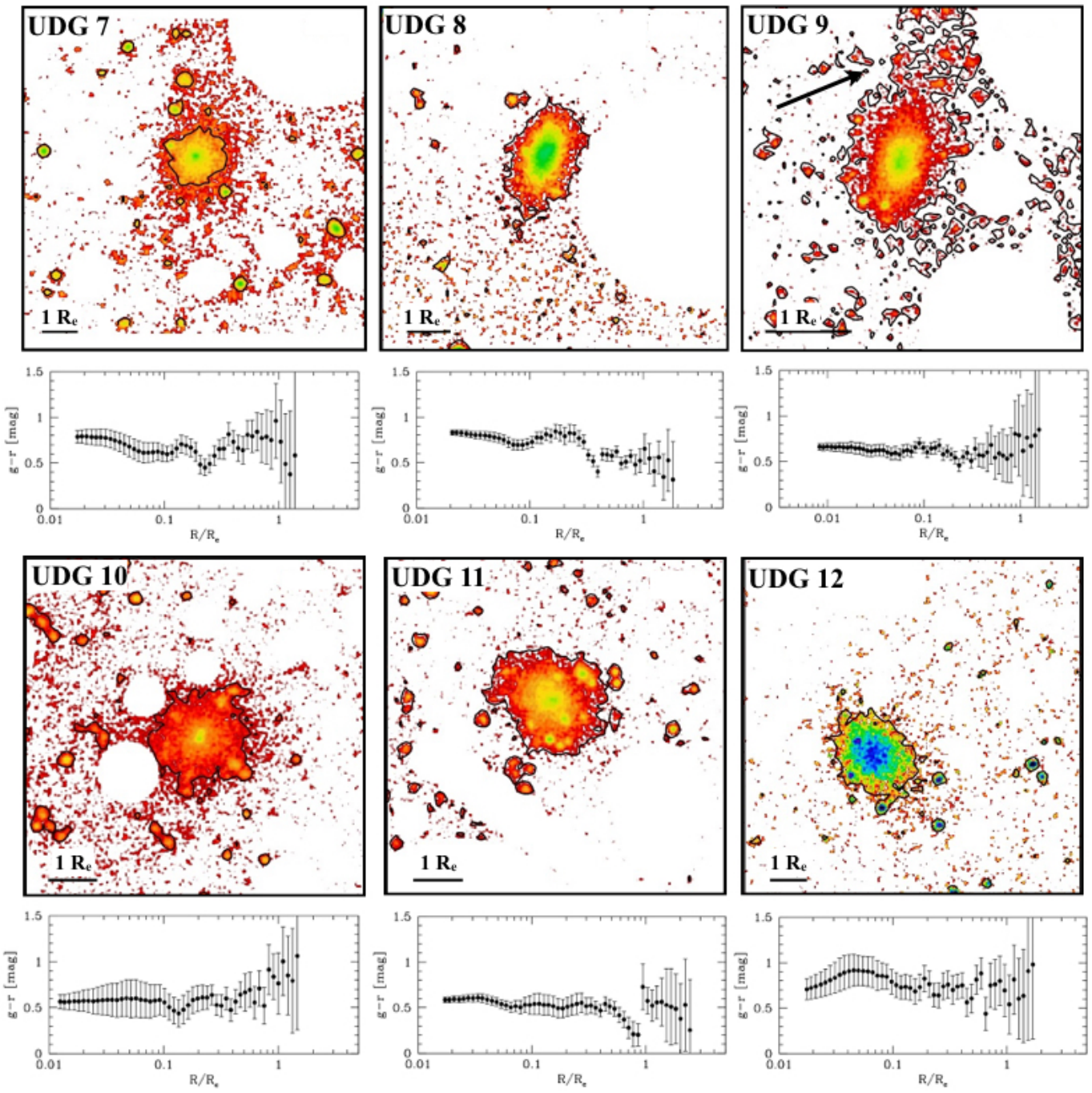


**Fig. 3.** Same as Fig. 2. The black arrow in the image of UDG 9 indicates the tidal tail described in the text.

GCs, which is done using the empirical relation $\log[M_{\rm h}] = 9.68 + 1.01 \times \log[N_{\rm GC}]$ (Burkert & Forbes 2020), and (ii) the GC's specific frequency[4] $S_N = N_{\rm GC} 10^{0.4[M_v+15]}$ . Values for both quantities are given in Table 3. The level of uncertainty on $N_{\rm GC}$ and the number of GC systems consistent with $N_{\rm GC} = 0$ for half of UDGs in the sample imply that our estimated $M_{\rm h}$ and $S_N$ suffer from correspondingly large uncertainties, and are in most cases formally consistent with zero. In future works, with more detailed characterisation of the GC's population extended over the survey area, we will be able to perform a more refined analysis of the GC numbers.

## 3. Results: UDGs structure and mass content

The colour-magnitude diagram (CMD) of the full sample of LSB galaxies and UDGs visually identified is shown in Fig. 5. The figure also includes the colour-magnitude relations derived by Misgeld et al. (2008) for giant and dwarf galaxies in Hydra I. In this plane, based on the error estimates, 25 out of 27 LSB galaxies match the plotted sequence.

In the range of magnitudes $M_r \simeq -15.5$ mag to $M_r \simeq -13.5$ mag, the $g$–$r$ colours of UDGs are consistent with the

[4] The $V$-magnitude and, therefore, the colour transformation from $g$–$r$ to $V$–$I$, are derived by assuming the equations given by Kostov & Bonev (2018).

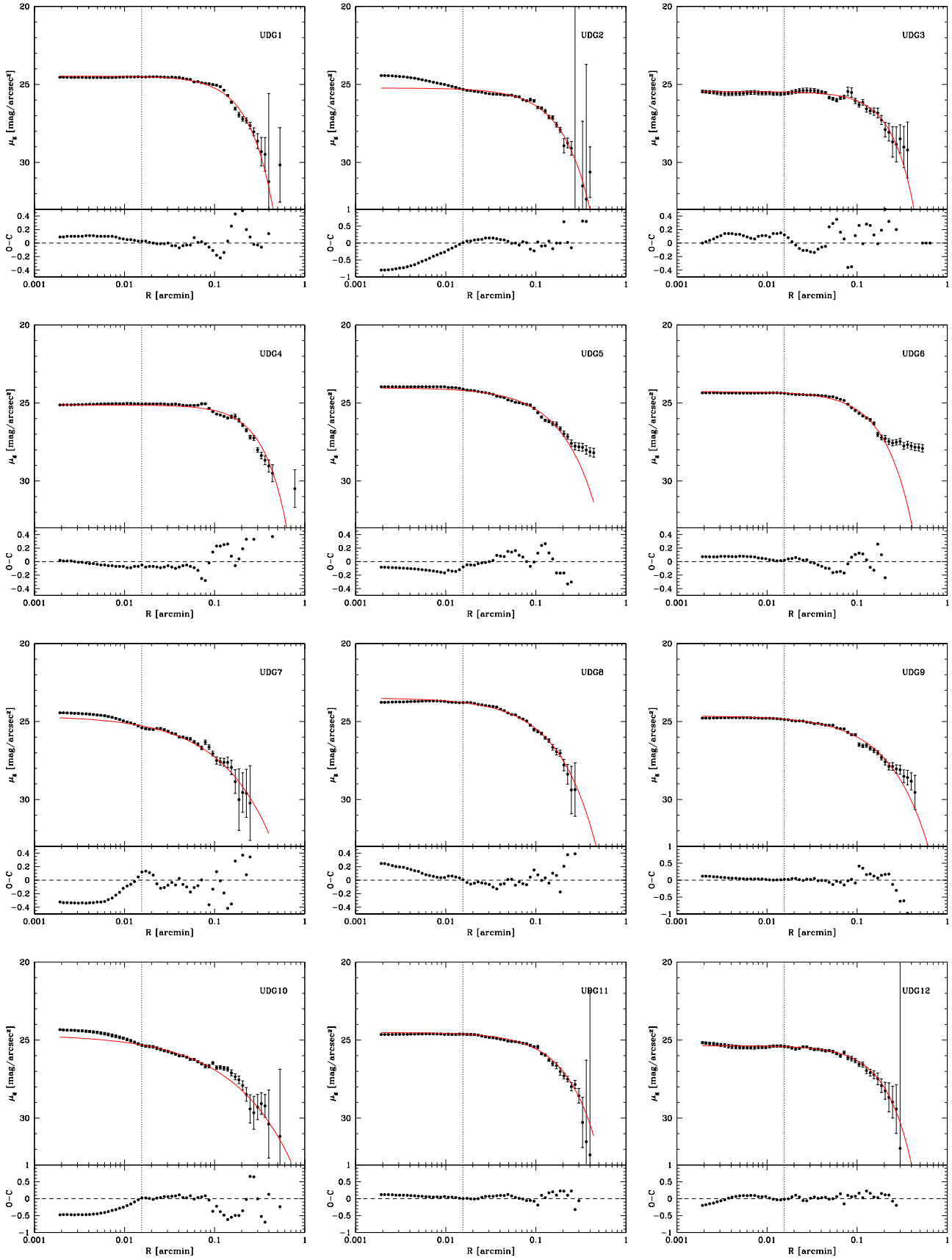


**Fig. 4.** Azimuthally averaged surface brightness profiles in the *g* band for the UDGs candidates (*top panels*). The red line indicates the best fit of the azimuthally averaged surface brightness profile derived from the 2D fit of the light distribution, using GALFIT. The vertical dotted line indicates the inner regions excluded from the fit, inside the seeing disc. The residuals of the fit are shown in the *lower panels*.

**Table 3.** Globular cluster candidates and halo mass estimates for the UDGs.

| ID | $N_{GC}$ ($\leq 1.5\,R_e$) | $N_{GC}$ ($\leq 5\,R_e$) | $M_h$ $10^{10}\,M_\odot$ | $M/L_V$ $10^3$ | $S_N$ | Nuclear star cluster candidates |
|---|---|---|---|---|---|---|
| Hydra I-UDG 1 | $0 \pm 1$ | $0 \pm 2$ | ... | ... | ... | ... |
| Hydra I-UDG 2 | $7 \pm 3$ | $3 \pm 2$ | $1.4 \pm 0.9$ | 0.43 | $7 \pm 5$ | $m_g \sim 24.2$, and ~25.2, both within $R_{proj} = 1$ arcsec |
| Hydra I-UDG 3 | $15 \pm 6$ | $6 \pm 2$ | $3 \pm 1$ | 0.96 | $11 \pm 4$ | $m_g \sim 24.2$ at $R_{proj} \leq 1$ arcsec, $m_g \sim 22.5$ at $R_{proj} \leq 7$ arcsec |
| Hydra I-UDG 4 | $2 \pm 1$ | $3 \pm 4$ | $1 \pm 1$ | 0.034 | $2 \pm 2$ | ... |
| Hydra I-UDG 5 | $0 \pm 1$ | $0 \pm 1$ | ... | ... | ... | ... |
| Hydra I-UDG 6 | $0 \pm 1$ | $0 \pm 1$ | ... | ... | ... | ... |
| Hydra I-UDG 7 | $3 \pm 1$ | $3 \pm 2$ | $1.4 \pm 0.9$ | 0.25 | $13 \pm 8$ | $m_g \sim 26.2$ at $R_{proj} \leq 1''$ |
| Hydra I-UDG 8 | $0 \pm 1$ | $0 \pm 0$ | ... | ... | ... | ... |
| Hydra I-UDG 9 | $7 \pm 3$ | $10 \pm 8$ | $5 \pm 4$ | 0.40 | $11 \pm 9$ | ... |
| Hydra I-UDG 10 | $0 \pm 1$ | $0 \pm 3$ | ... | ... | ... | Two partially blended sources at $R_{proj} \leq 1$ arcsec |
| Hydra I-UDG 11 | $7 \pm 3$ | $5 \pm 2$ | $2.4 \pm 0.9$ | 0.35 | $7 \pm 3$ | Diffuse nuclear source |
| Hydra I-UDG 12 | $0 \pm 1$ | $0 \pm 1$ | ... | ... | ... | ... |

**Notes.** Column 1 reports the name of the UDG candidate. Columns 2 and 3 give the total number of GC candidates inside $R = 1.5\,R_e$ and $5\,R_e$, respectively. Columns 4 and 5 report the halo mass and the $V$-band halo mass-to-light ratio, respectively. Column 6 lists the GC specific frequency derived from the total number of GCs inside $5\,R_e$. Column 7 provides some details on the presence of nuclear star clusters (NSC); if present, the $g$ magnitude and the projected galactocentric distance from the galaxy core, $R_{proj}$, are reported.

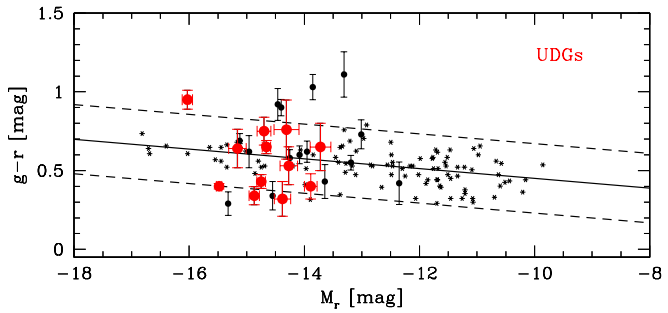


**Fig. 5.** colour-magnitude diagram (CMD) for the full sample of LSB galaxies (black points) detected in the VST Hydra I mosaic. Red filled circles indicate the UDG candidates. The solid black line is the CM relation for the Hydra I cluster galaxies derived by Misgeld et al. (2008, dashed lines indicate the $2\sigma$ scatter). The asterisks indicate dwarf galaxies from Misgeld et al. (2008).

known early-type dwarf galaxy population in Hydra I, with $0.3 \leq g{-}r \leq 0.8$ mag. Similar colours, in the same range of luminosity, were found for the dwarf galaxies in the Fornax cluster (Venhola et al. 2019), as well as for the UDGs in the Abell 186 cluster (Román & Trujillo 2017), which means $0.5 \leq g{-}r \leq 0.8$ mag.

The reddest and brightest LSB galaxy in the sample, UDG 4 ($g{-}r = 0.95 \pm 0.10$ mag, $M_r = -16.04$ mag, Table 1), being ~0.1 mag beyond the $2\sigma$ boundary of the CMD, might rather be a background galaxy. Unfortunately, the distance for this galaxy is unknown. However, even though we cannot derive any definitive conclusion on its membership, since this is one of the most extended and diffuse galaxies of the whole LSB sample (with $R_e = 2.64$ kpc, $\mu_0 = 24.86$ mag arcsec$^{-2}$ (see Table 1), it remains an interesting object to include in our analysis.

The detected LSB candidates and the selected UDGs are plotted on the $\mu_0 - R_e$ plane, in Fig. 6. In this figure, we also plot the dwarf galaxies from the Misgeld et al. (2008) catalogue. All our LSB galaxies are new candidates, fainter and more extended, with respect to the objects in that catalogue. Only one LSB galaxy in the Misgeld et al. (2008) catalogue, HCC 087, falls into the selection region of UDGs. However, it was described as a faint ($\mu_0 \sim 26.2$ mag arcsec$^{-2}$ in the $g$ band), tidally disrupted dwarf because of its peculiar S-shape (Koch et al. 2012).

In Fig. 6 (middle and upper panels), we examine the correlations between the Sersic $n$-exponent and average $g{-}r$ colours as a function of $R_e$, for both the new LSB galaxies (including UDGs) and the dwarf galaxies from Misgeld et al. (2008). Most of the LSB galaxies and UDGs have colours that are comparable with those observed for cluster dwarfs, in the range of $g{-}r \sim 0.3{-}0.8$ mag. The Sersic $n$-exponents derived for galaxies in the sample presented here are consistent with the values for dwarfs ($n \sim 0.4{-}1.8$).

In Fig. 7, we show the distributions of the structural parameters (axial ratio $q$, Sersic index $n$, effective radius $R_e$ and central surface brightness $\mu_0$) derived for the UDG candidates in Hydra I cluster. They are consistent with those obtained for the UDGs in the Coma and Abell 168 clusters (Yagi et al. 2016; Román & Trujillo 2017), as well as with the results from more recent studies on UDGs in clusters of galaxies (Lee et al. 2020). As observed in other clusters, UDGs in Hydra I seem to be quite round systems, with $q$ in the range of 0.6–0.8, and most of them have a Sersic index $n \sim 0.5{-}1.0$, with an average value $n \sim 0.8$, and only a few UDGs have larger values for the $n$-exponent.

### 3.1. Structure and colour distribution

The deep VST images allow us to map the surface brightness distribution of the UDGs down to $\mu_g \sim 27{-}29$ mag arcsec$^{-2}$ (see Figs. 2 and 3). At these depths, we are able to study the galaxy outskirts and detect any signs of tidal features.

This seems to be the case of UDG 4, UDG 6, and UDG 9. The structure of UDG 4 is quite irregular in the outskirts, showing a clear over-density of light on the SW side. Although UDG 6 and UDG 9 have more regular spheroidal-like shapes, they present tidal features in the outskirts and are located towards the central part of the Hydra I cluster, as shown by the brighter X-ray emission (Hayakawa et al. 2004, 2006). We describe their outer morphologies hereafter: UDG 6 has spiral-like tails on the SW side. It is located north of the cluster core (see Fig. 1), where tidal forces might be acting on the galaxies: HCC 005, an S0 galaxy with a prominent tidal tail, is to the west, and it is near the tidally disrupted dwarf galaxy HCC 087 (Koch et al. 2012). Furthermore, UDG 9 has an extended tail (~0.5 arcmin) on the NW

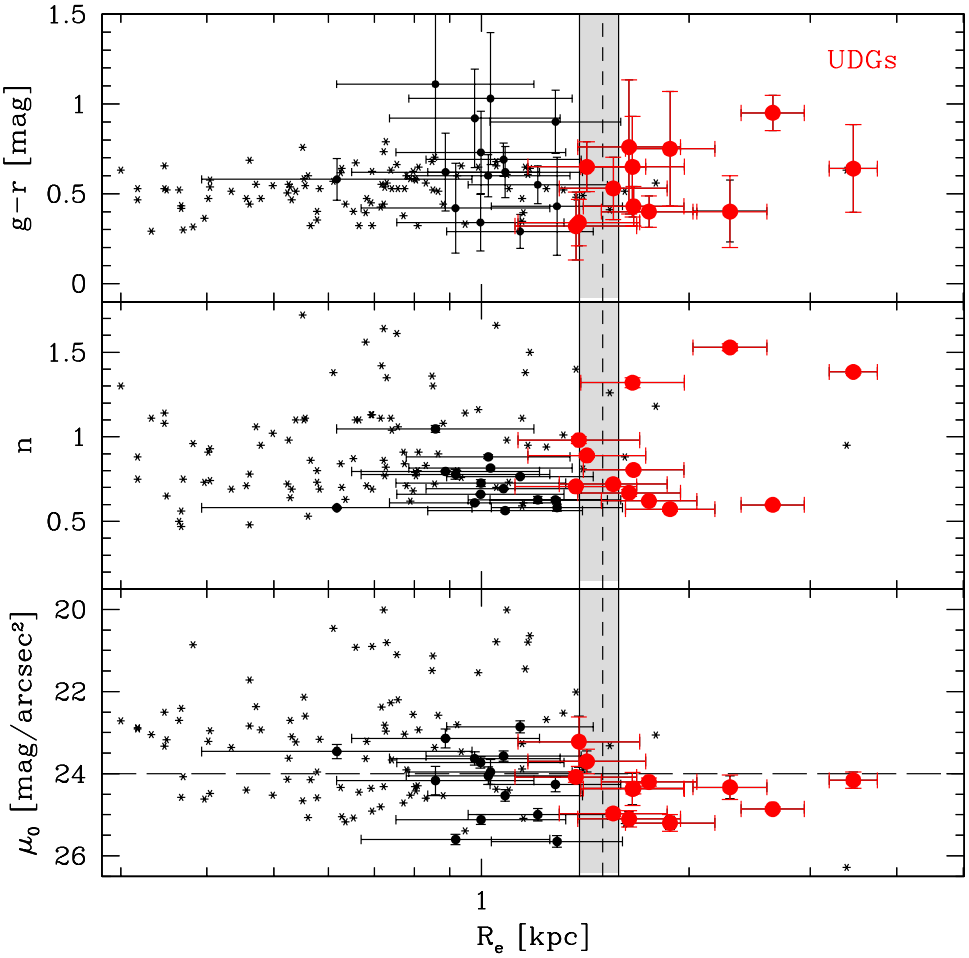


**Fig. 6.** Structural and photometric parameters for the newly discovered LSB galaxies (dots with error-bars) in Hydra I as a function of the effective radius. The UDGs are marked with red circles. The UDG definition criteria, $R_e \geq 1.5$ kpc and $\mu_0 \geq 24$ mag arcsec$^{-2}$ (van Dokkum et al. 2015), are shown by the dashed lines. The shaded box indicates the lower and upper limits on the selection criteria on $R_e$ due to the uncertainty on the distance (i.e., $R_e \pm 0.12$ kpc). The asterisks are dwarf galaxies in Hydra I from Misgeld et al. (2008). The only LSB galaxy in Misgeld et al. (2008) catalogue falling in the region of UDGs is HCC 087. As explained in the text, this was described as a faint tidally disrupting dwarf because of its peculiar *S*-shape (Koch et al. 2012).

side that protrudes from the elongated isophotes of this galaxy in this direction. Next, UDG 9 is projected on the SE region of the cluster core, inside the infalling sub-group dominated by the bright spiral galaxy, NGC 3312, where the effect of ram pressure is visible in the form of several extended blue filaments. Tidal features around UDGs have also been observed in other clusters for objects that are close to major galaxies (Mihos et al. 2015; Lee et al. 2017). Such features would support the tidal interaction formation scenario (Amorisco 2018; van Dokkum et al. 2016; Di Cintio et al. 2017; Carleton et al. 2019; Sales et al. 2020).

Close to the centres of UDG 1 and UDG 5, there are signs of an ongoing interaction. In UDG 1, we detected a spiral-like feature that ends with a bright nucleus in the west. In UDG 5, there is a small system on the SE side that seems to be merging into the galaxy core.

The $g-r$ colour profiles are, on average, flat inside $1\,R_e$ for most of the UDGs, in the range of 0.3−0.7 mag (see Figs. 2 and 3). In the cases of UDG 4, UDG 7, and UDG 8, we see redder colours towards the centre, reaching $g-r \sim 0.8$ mag. Some other UDGs (UDG 2, UDG 3, UDG 6, and UDG 12) instead have bluer colours in the centre, decreasing by ∼0.2 mag with respect to the outer regions.

### 3.2. Compact sources in UDGs

For most of the UDGs we were able to to identify compact sources in their surroundings (see Sect. 2.2). Overall, we found that most of the UDGs host only a few GCs, with $3 \leq N_{GC} \leq 10$ for six out of 12 UDG candidates inside $5\,R_e$ (see Table 3). Moreover, UDG 3 and UDG 9 are the two objects with the largest number of GCs, with $N_{GC} = 6$ and $N_{GC} = 10$ inside $5\,R_e$, respectively. For six UDGs, the predicted number of GCs is consistent with zero, within both $1.5\,R_e$ and $5\,R_e$.

As observed in previous studies with larger samples, we found that for most of the UDGs in Hydra I, the GCs specific frequency $S_N$ is consistent with the upper limits derived for dwarf galaxies of comparable luminosity (see top panel of Fig. 8), and it is fully consistent with values derived for UDGs in the Coma cluster (see van Dokkum et al. 2017; Amorisco et al. 2018; Lim et al. 2018; Forbes et al. 2020a). The galaxies with the largest $S_N$ (∼11−13) are UDG 3, UDG 7, and UDG 9. Two of them, UDG 7 and UDG 9, are close in projection to the cluster core. While the actual $S_N$ for our targets needs to be confirmed through follow-up studies, this appears to be in agreement with suggestions from Lim et al. (2018), who reported, although with a large scatter, a trend between $S_N$ and environment, where UDGs with higher $S_N$ are located in the densest cluster regions.

Consistently with previous results, about 30% of the UDGs in our sample show a nuclear star cluster (NSC) candidate, which are the brightest "GCs" in their respective GC systems and are located very close to the galaxy centre. As a comparison, the nucleation fraction is about 23% for UDGs in Coma (Lim et al. 2018). The two NSC candidates in UDG 2 are very close to the galaxy centre (≤1 arcsec) and have a $m_g \simeq 24.2$ and 25.2 mag. The UDG 3 hosts an NSC candidate within 1 arcsec from the centre, with $m_g \simeq 24.2$ mag, though also a second, brighter $m_g \simeq 22.2$ mag, source is consistent with a star cluster located

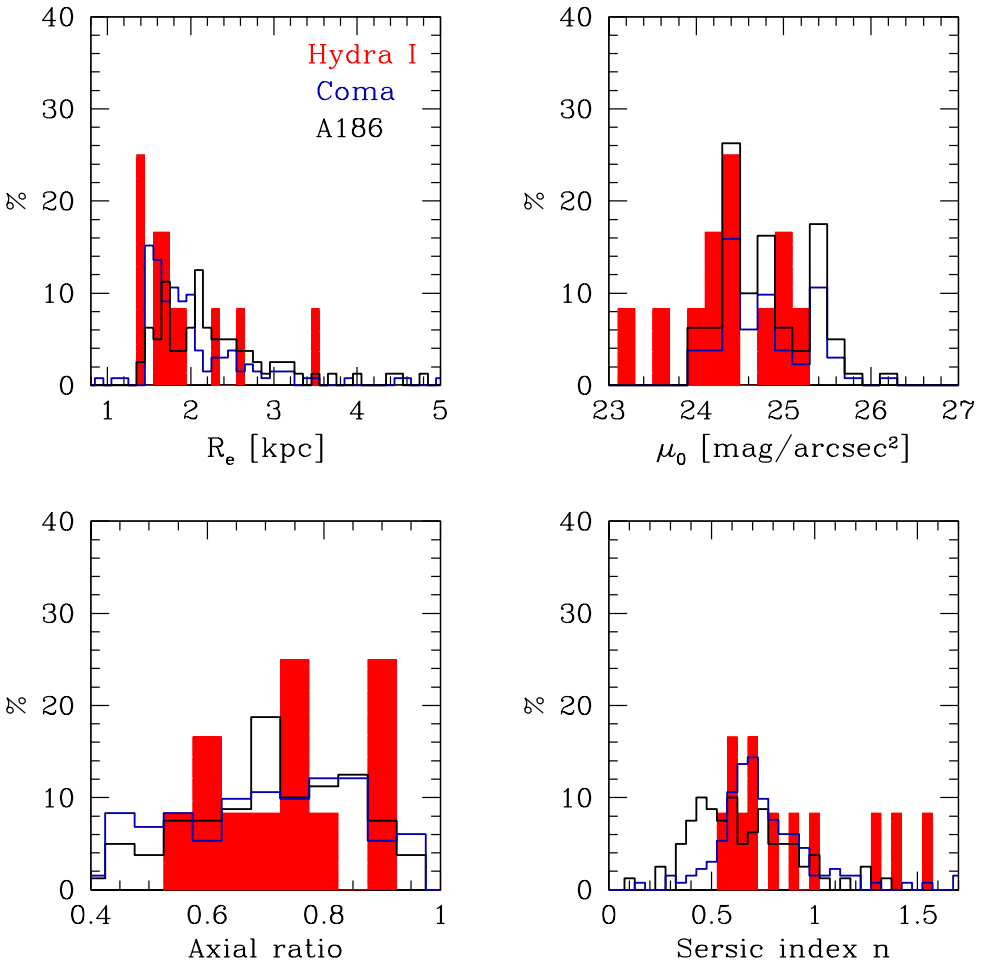


**Fig. 7.** Distribution of the structural parameters for the UDG candidates in Hydra I(filled red histogram). Axial ratio (*lower-left panel*), Sersic index $n$ (*lower right panel*), effective radius $R_e$ (*top-left panel*), and central surface brightness $\mu_0$ (*top-right panel*) are compared with the same parameters derived for the UDGs in the Abell 168 cluster (black line) by Román & Trujillo (2017) and in Coma cluster (blue line) by Yagi et al. (2016).

at ∼7 arcsec from the galaxy centre (see also Fig. 2). The candidate NSC in UDG 7 is in the galaxy centre and has a relatively faint g-band magnitude of $m_g \simeq 26.2$ mag. In UDG 10, there are two close sources within the galaxy centre that could also be classified as NSCs.

### 3.3. Stellar mass versus DM content

The $g-r$ colours and absolute magnitudes in the $r$ band ($M_r$) are used to derive the stellar mass for all UDG candidates, using the relation given by Into & Portinari (2013). Values are listed in Table 1. Most of the UDGs have stellar masses in the range of $10^7-10^8\,M_\odot$. The halo mass range, estimated from the total number of GCs (see Sect. 2.2) for half of the UDGs in the sample, is $1-3\times10^{10}\,M_\odot$ (see Table 3). By propagating the large uncertainties on $N_{GC}$, the error estimate on $M_h$ is quite large, ranging from 40% to 80%. The mass-to-light ratio derived for these six UDGs is in the range of $250 \le M/L_V \le 10^3$. Concerning UDG 3, which is one of the galaxies with the highest $S_N$ (see Tables 1 and 3), it has the largest $M/L_V \sim 10^3$. The lowest $M/L_V \sim 34$ is derived for UDG 4, which is also the system with the lowest $S_N \sim 2$. Therefore, if UDG 4 is confirmed as a Hydra I member in future investigations, it might have a low amount of DM compared to what is expected for its total luminosity. However, the estimated $N_{GC}$ in this case is consistent with zero within $1\sigma$, therefore, given its high luminosity, the absence of GCs would point towards this galaxy being a background object.

In the halo mass versus stellar mass relation, within the uncertainties, the UDGs in Hydra I have halo masses consistent with normal galaxies of comparable luminosity, as well as with UDGs in the Coma cluster (see lower panel of Fig. 8).

## 4. Summary and concluding remarks

From the visual inspection of a new mosaic image obtained for the Hydra I cluster, with VST $g$ and $r$ imaging, we identified a sample of 27 LSB galaxies, which are not included in any previous catalogue. Twelve LSB galaxies were selected as UDG candidates. This is the first sample of UDGs in the Hydra I cluster.

Since the nature and formation of the UDGs is still poorly constrained, even from works based on larger samples, this study aims at extending such studies to the Hydra I cluster, which so far had limited studies in the low surface brightness regime.

We find that most of the UDGs have stellar masses in the range of $10^7-10^8\,M_\odot$. Given the limitations of a reliable GC selection based on two relatively close optical bands only, we find that half the UDG candidates have a total population of GCs consistent with zero ($N_{GCs} \sim 0$). The other half of the UDGs seem to have a standard or low DM content, with halo mass $\le 10^{10}\,M_\odot$, which is comparable to dwarf galaxies of similar luminosity.

In conclusion, even considering the low number of UDGs, the analysis presented in this work might suggest that most of the UDGs in the Hydra I cluster resemble diffuse dwarf-like galaxies in terms of their stellar mass and DM content, with comparable colours to those of dwarf galaxies in the same range of luminosity. This result, however, suffers from the large uncertainties coming from the $N_{GCs}$ estimates. In particular, due to the low

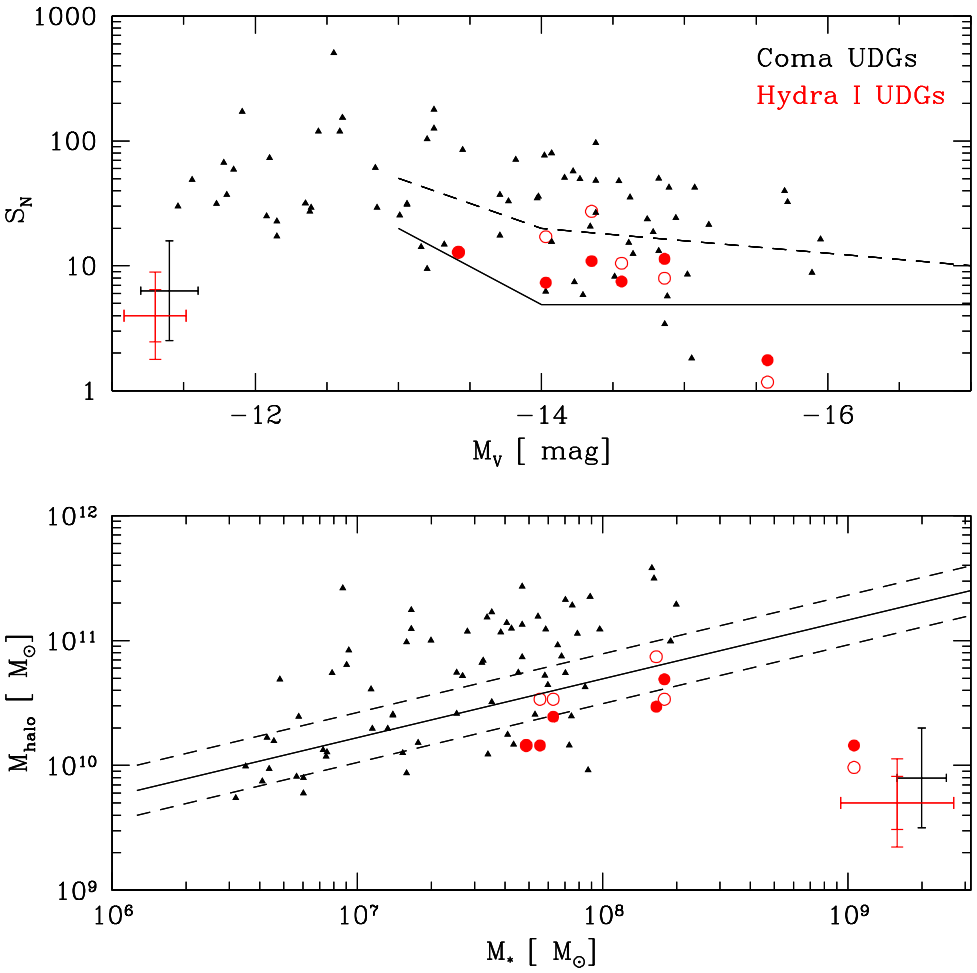


**Fig. 8.** *Upper panel*: GCs specific frequency $S_N$ versus $V$-band absolute magnitude for the Hydra I UDG sample (red), compared with the UDGs in the Coma cluster (black triangles) by Forbes et al. (2020a). For the UDGs in Hydra I, the filled red circles are for values derived inside $5R_e$, empty red circles for values derived inside $1.5\,R_e$. The solid line shows the mean locus of dwarf galaxies, the dotted line represents the upper $2\sigma$ bound (see also Fig. 4 in Lim et al. 2018). The average uncertainties on both samples are shown in the lower left corner. *Lower panel*: Halo mass versus stellar mass. The halo for the UDGs in Hydra I is derived from the total number of GCs, using the scaling relation by Burkert & Forbes (2020), see text for details. Symbols are the same as in upper panel. The average uncertainties on both samples are plotted in the lower right corner. The black solid line is the extrapolated stellar mass-halo mass relation for normal galaxies by Rodríguez-Puebla et al. (2017), with a scatter of ±0.2 dex (dashed lines).

number of tracers and large contamination from foreground and background objects, the DM estimate from GCs is quite uncertain. Follow-up studies, which include both deep multi-band imaging data, preferably including near-IR bands, coupled with a more detailed analysis over the entire area surveyed (which is in progress), and integral field spectroscopy, will substantially help in reducing such uncertainty. Future systematic searches for UDGs and their analysis in this cluster will be fundamental to checking whether DM-dominated systems are also present, and, therefore, to putting further observational constraints on the existence of two distinct formation channels for this class of galaxies.

Taking into account the virial mass of the Hydra I cluster ($2\times10^{14}\,M_\odot$, Girardi et al. 1998), from the abundance-halo mass relation (Janssens et al. 2019) we expect up to 100 UDGs inside the cluster virial radius. A follow-up study, in which the UDG detection is not carried out visually, but using automated tools already tested on the Fornax galaxy cluster (Venhola et al. 2019), is in progress.

This work is part of a large programme to study the internal structure, formation history, evolution and DM fraction in UDGs across different environments identified from the deep, wide-field imaging data of VEGAS. We aim to identify and study a large number (~1300) of UDGs using automatic LSB detection tools on the entire VEGAS sample, which includes about 30 groups and 10 clusters of galaxies for a total covered area of more than ~100 deg$^2$. The new sample will almost double the number of studied UDGs and will have a legacy value for future follow-up imaging and spectroscopic observations.

*Acknowledgements.* This work is based on visitor mode observations taken at the ESO La Silla Paranal Observatory within the VST Guaranteed Time Observations, Programme ID: 099.B-0560(A). We thank the anonymous referee for his/her useful suggestions that helped to improve the paper. EI acknowledge financial support from the ESO during the science visit at the Garching HQ, from September 1st, 2019 up to August 2020. MS and EI acknowledge finacial support from the VST project (P. I. P. Schipani). Authors wish to thank ESO for the financial contribution given for the visitor mode runs at the ESO La Silla Paranal Observatory. GD acknowledges support from CONICYT project Basal AFB-170002.

## References

Alabi, A., Ferré-Mateu, A., Romanowsky, A. J., et al. 2018, MNRAS, 479, 3308
Amorisco, N. C. 2018, MNRAS, 475, L116
Amorisco, N. C., & Loeb, A. 2016, MNRAS, 459, L51
Amorisco, N. C., Monachesi, A., Agnello, A., & White, S. D. M. 2018, MNRAS, 475, 4235
Arnaboldi, M., Ventimiglia, G., Iodice, E., Gerhard, O., & Coccato, L. 2012, A&A, 545, A37
Barbosa, C. E., Arnaboldi, M., Coccato, L., et al. 2018, A&A, 609, A78
Beasley, M. A., & Trujillo, I. 2016, ApJ, 830, 23
Beasley, M. A., Romanowsky, A. J., Pota, V., et al. 2016, ApJ, 819, L20
Bertin, E., & Arnouts, S. 1996, A&AS, 117, 393
Burkert, A., & Forbes, D. A. 2020, AJ, 159, 56
Cantiello, M., Capaccioli, M., Napolitano, N., et al. 2015, A&A, 576, A14
Cantiello, M., D'Abrusco, R., Spavone, M., et al. 2018a, A&A, 611, A93
Cantiello, M., Grado, A., Rejkuba, M., et al. 2018b, A&A, 611, A21
Cantiello, M., Venhola, A., Grado, A., et al. 2020, A&A, 639, A136
Capaccioli, M., Spavone, M., Grado, A., et al. 2015, A&A, 581, A10
Carleton, T., Errani, R., Cooper, M., et al. 2019, MNRAS, 485, 382
Caso, J. P., De Bórtoli, B. J., Ennis, A. I., & Bassino, L. P. 2019, MNRAS, 488, 4504
Christlein, D., & Zabludoff, A. I. 2003, ApJ, 591, 764

Coccato, L., Gerhard, O., Arnaboldi, M., & Ventimiglia, G. 2011, A&A, 533, A138
Danieli, S., van Dokkum, P., Conroy, C., Abraham, R., & Romanowsky, A. J. 2019, ApJ, 874, L12
Di Cintio, A., Brook, C. B., Dutton, A. A., et al. 2017, MNRAS, 466, L1
Fensch, J., van der Burg, R. F. J., Jeřábková, T., et al. 2019, A&A, 625, A77
Ferré-Mateu, A., Alabi, A., Forbes, D. A., et al. 2018, MNRAS, 479, 4891
Forbes, D. A. 2017, MNRAS, 472, L104
Forbes, D. A., Gannon, J., Couch, W. J., et al. 2019, A&A, 626, A66
Forbes, D. A., Dullo, B. T., Gannon, J., et al. 2020a, MNRAS, 494, 5293
Forbes, D. A., Alabi, A., Romanowsky, A. J., Brodie, J. P., & Arimoto, N. 2020b, MNRAS, 492, 4874
Girardi, M., Borgani, S., Giuricin, G., Mardirossian, F., & Mezzetti, M. 1998, ApJ, 506, 45
Girardi, L., Groenewegen, M. A. T., Hatziminaoglou, E., & da Costa, L. 2005, A&A, 436, 895
Grado, A., Capaccioli, M., Limatola, L., & Getman, F. 2012, Mem. Soc. Astron. It. Suppl., 19, 362
Gu, M., Conroy, C., Law, D., et al. 2018, ApJ, 859, 37
Hanes, D. A. 1977, MNRAS, 180, 309
Hayakawa, A., Furusho, T., Yamasaki, N. Y., Ishida, M., & Ohashi, T. 2004, PASJ, 56, 743
Hayakawa, A., Hoshino, A., Ishida, M., et al. 2006, PASJ, 58, 695
Hilker, M., Richtler, T., Barbosa, C. E., et al. 2018, A&A, 619, A70
Into, T., & Portinari, L. 2013, MNRAS, 430, 2715
Iodice, E., Capaccioli, M., Grado, A., et al. 2016, ApJ, 820, 42
Iodice, E., Spavone, M., Capaccioli, M., et al. 2019, A&A, 623, A1
Iodice, E., Spavone, M., Cattapan, A., et al. 2020, A&A, 635, A3
Janssens, S. R., Abraham, R., Brodie, J., Forbes, D. A., & Romanowsky, A. J. 2019, ApJ, 887, 92
Kartha, S. S., Forbes, D. A., Spitler, L. R., et al. 2014, MNRAS, 437, 273
Koch, A., Burkert, A., Rich, R. M., et al. 2012, ApJ, 755, L13
Koda, J., Yagi, M., Yamanoi, H., & Komiyama, Y. 2015, ApJ, 807, L2
Kostov, A., & Bonev, T. 2018, BlgAJ, 28, 3
Kron, R. G. 1980, ApJS, 43, 305
Lee, M. G., Kang, J., Lee, J. H., & Jang, I. S. 2017, ApJ, 844, 157
Lee, J. H., Kang, J., Lee, M. G., & Jang, I. S. 2020, ApJ, 894, 75
Leisman, L., Haynes, M. P., Janowiecki, S., et al. 2017, ApJ, 842, 133
Lim, S., Peng, E. W., Côté, P., et al. 2018, ApJ, 862, 82
Martín-Navarro, I., Romanowsky, A. J., Brodie, J. P., et al. 2019, MNRAS, 484, 3425
Mihos, J. C., Durrell, P. R., Ferrarese, L., et al. 2015, ApJ, 809, L21
Misgeld, I., Mieske, S., & Hilker, M. 2008, A&A, 486, 697
Misgeld, I., Mieske, S., Hilker, M., et al. 2011, A&A, 531, A4
Müller, O., Jerjen, H., & Binggeli, B. 2018, A&A, 615, A105
Peng, E. W., & Lim, S. 2016, ApJ, 822, L31
Peng, Y.-J., Lilly, S. J., Kovač, K., et al. 2010, ApJ, 721, 193
Peng, E. W., Ferguson, H. C., Goudfrooij, P., et al. 2011, ApJ, 730, 23
Prole, D. J., van der Burg, R. F. J., Hilker, M., & Davies, J. I. 2019a, MNRAS, 488, 2143
Prole, D. J., Hilker, M., van der Burg, R. F. J., et al. 2019b, MNRAS, 484, 4865
Rejkuba, M. 2012, Ap&SS, 341, 195
Richtler, T., Salinas, R., Misgeld, I., et al. 2011, A&A, 531, A119
Robin, A. C., Reylé, C., Derrière, S., & Picaud, S. 2003, A&A, 409, 523
Rodríguez-Puebla, A., Primack, J. R., Avila-Reese, V., & Faber, S. M. 2017, MNRAS, 470, 651
Román, J., & Trujillo, I. 2017, MNRAS, 468, 703
Rong, Y., Guo, Q., Gao, L., et al. 2017, MNRAS, 470, 4231
Ruiz-Lara, T., Beasley, M. A., Falcón-Barroso, J., et al. 2018, MNRAS, 478, 2034
Sales, L. V., Navarro, J. F., Peñafiel, L., et al. 2020, MNRAS, 494, 1848
Schipani, P., Noethe, L., Arcidiacono, C., et al. 2012, J. Opt. Soc. Am. A, 29, 1359
Schlegel, D. J., Finkbeiner, D. P., & Davis, M. 1998, ApJ, 500, 525
Shi, D. D., Zheng, X. Z., Zhao, H. B., et al. 2017, ApJ, 846, 26
Spavone, M., Iodice, E., Capaccioli, M., et al. 2018, ApJ, 864, 149
Tremmel, M. J., Wright, A., Munshi, F., et al. 2019, in Am. Astron. Soc. Meeting Abstr., 233, 416.04
van der Burg, R. F. J., Hoekstra, H., Muzzin, A., et al. 2017, A&A, 607, A79
van Dokkum, P. G., Romanowsky, A. J., Abraham, R., et al. 2015, ApJ, 804, L26
van Dokkum, P., Abraham, R., Brodie, J., et al. 2016, ApJ, 828, L6
van Dokkum, P., Abraham, R., Romanowsky, A. J., et al. 2017, ApJ, 844, L11
van Dokkum, P., Wasserman, A., Danieli, S., et al. 2019a, ApJ, 880, 91
van Dokkum, P., Danieli, S., Abraham, R., Conroy, C., & Romanowsky, A. J. 2019b, ApJ, 874, L5
Venhola, A., Peletier, R., Laurikainen, E., et al. 2018, A&A, 620, A165
Venhola, A., Peletier, R., Laurikainen, E., et al. 2019, A&A, 625, A143
Ventimiglia, G., Arnaboldi, M., & Gerhard, O. 2011, A&A, 528, A24
Villegas, D., Jordán, A., Peng, E. W., et al. 2010, ApJ, 717, 603
Wright, A. C., Tremmel, M., Brooks, A. M., et al. 2020, MNRAS, submitted, ArXiv e-prints [arXiv:2005.07634]
Yagi, M., Koda, J., Komiyama, Y., & Yamanoi, H. 2016, ApJS, 225, 11
Yozin, C., & Bekki, K. 2015, MNRAS, 452, 937